metals

MDPI

Article

Sensitivity Analysis of Oxide Scale Influence on General Carbon Steels during Hot Forging

Bernd-Arno Behrens [1], Alexander Chugreev [1], Birgit Awiszus [2], Marcel Graf [2], Rudolf Kawalla [3], Madlen Ullmann [3], Grzegorz Korpala [3] and Hendrik Wester [1,*]

[1] Institute of Forming Technology and Machines, Leibniz Universität Hannover, 30823 Garbsen, Germany; behrens@ifum.uni-hannover.de (B.-A.B.); chugreev@ifum.uni-hannover.de (A.C.)
[2] Professorship Virtual Production Engineering, Technische Universität Chemnitz, 09126 Chemnitz, Germany; birgit.awiszus@mb.tu-chemnitz.de (B.A.); marcel.graf@mb.tu-chemnitz.de (M.G.)
[3] Institute of Metal Forming, Technische Universität Freiberg, 09599 Freiberg, Germany; Rudolf.Kawalla@imf.tu-freiberg.de (R.K.); Madlen.Ullmann@imf.tu-freiberg.de (M.U.); Grzegorz.Korpala@imf.tu-freiberg.de (G.K.)
* Correspondence: wester@ifum.uni-hannover.de; Tel.: +49-511-762-3405

Received: 8 December 2017; Accepted: 12 February 2018; Published: 14 February 2018

Abstract: Increasing product requirements have made numerical simulation into a vital tool for the time- and cost-efficient process design. In order to accurately model hot forging processes with finite, element-based numerical methods, reliable models are required, which take the material behaviour, surface phenomena of die and workpiece, and machine kinematics into account. In hot forging processes, the surface properties are strongly affected by the growth of oxide scale, which influences the material flow, friction, and product quality of the finished component. The influence of different carbon contents on material behaviour is investigated by considering three different steel grades (C15, C45, and C60). For a general description of the material behaviour, an empirical approach is used to implement mathematical functions for expressing the relationship between flow stress and dominant influence variables like alloying elements, initial microstructure, and reheating mode. The deformation behaviour of oxide scale is separately modelled for each component with parameterized flow curves. The main focus of this work lies in the consideration of different materials as well as the calculation and assignment of their material properties in dependence on current process parameters by application of subroutines. The validated model is used to carry out the influence of various oxide scale parameters, like the scale thickness and the composition, on the hot forging process. Therefore, selected parameters have been varied within a numerical sensitivity analysis. The results show a strong influence of oxide scale on the friction behaviour as well as on the material flow during hot forging.

Keywords: hot forging; finite-element; oxide scale

1. Introduction

In the field of bulk metal forming, hot forging is a widely-used process for the production of high-performance parts with complex shapes. The preheating of semi-finished parts to temperatures above 800 °C leads to a significant reduction in required forming forces as well as an increase in the material formability. Furthermore, the process efficiency can be increased by the use of process heat energy for a direct thermomechanical treatment to produce parts with locally-adapted properties [1]. However, a major disadvantage is the appearance of oxidation effects on the preheated steel surfaces. The scale layer itself has an inhomogeneous structure. On a steel surface, it typically consists of three different iron oxides, namely wuestite, magnetite, and haematite. The development and growth of these oxides depend on the steel matrix properties like the used alloying concept and surface quality

as well as the oxidation time, atmosphere, and temperature. The formation of oxide scale leads to material losses of up to 3% by weight and requires further process steps for removal and rework. During the forging process, the presence of oxide scale influences friction as well as material flow and can lead to an increase in die wear [2]. The tooling and setup cost up to 15% of total production costs in bulk metal forming and extensive investigations on tool failure have shown that more than 70% is caused by die wear [3]. Therefore, die wear has a decisive influence on the entire efficiency of a hot forging process [4].

The oxidation process on heated steel surfaces is significantly influenced by alloying elements. The influence of different alloying elements on the formation of an oxide scale layer is described in [5]. Comparison of Si-steel with IF-steel and S355-steel have shown that the alloying elements Si and P lead to a delayed oxidation at lower temperatures and to a significantly increased oxidation rate for temperatures above 1100 °C. Previous studies investigated the influence of carbon content on the formation of oxide scale and have shown a relationship between temperature, carbon content, and growth of oxide scale. Temperatures higher than 700 °C in combination with a high carbon content lead to a decrease in oxide scale layer thickness [6,7]. The composition of oxide scale is variable. The oxidation behaviour of pure iron in air and oxygen atmosphere has been examined in numerous studies [8,9]. They pointed out that the classic oxide scale structure at temperatures above 700 °C consists of an extremely thin cover layer of haematite, a thin intermediate layer of magnetite, and a thick inner layer of wuestite directly on the steel surface. With a decrease in temperature below 650 °C, the layer thickness of magnetite and haematite increases whereas that of wuestite decreases. Until about 580 °C, wuestite is still the major phase. A further decrease in temperature below 570 °C leads to an unstable wuestite layer. Thus the oxide scale layer consists of two iron oxides, a thick layer of magnetite with about 80 wt %, and a thin haematite cover layer [10]. In the temperature range between 700 °C and 1250 °C, the oxide scale composition is nearly constant with a ratio of 1:4:95 for the layers of haematite, magnetite, and wuestite, respectively [11].

Experimental studies in the temperature range between 900 °C and 1200 °C have shown strong varying forming behaviour of the different iron oxides wuestite, magnetite, and haematite, which build up the typical oxide scale layer on general steel. The yield stresses are observed to be strongly temperature-dependent as known for metals. The yield stress of wuestite has been found to be low as compared to magnetite, whereas the highest bearable strain was found for wuestite. Maximum yield stress has been observed for haematite. Moreover, it has been found to be the hardest oxide scale component at room temperature with a Vickers hardness of 1000 HV10 as compared to magnetite (600 HV10) and wuestite (400 HV10). Furthermore, the investigations have shown a significant and partly contrary influence of the strain rate on the forming behaviour. Contrary to haematite, magnetite and wuestite show an increase in yield stress with increasing strain rate [12,13]. Further investigations on synthesized iron oxides at high temperatures have shown a strong dependency of hardness on temperature. The hardness of all the oxides decreases with an increase in temperature, whereby the strongest reduction was observed for magnetite and haematite [14].

The development of an oxide scale layer on the steel surface in a metal forming process results in changes in surface properties. In particular, friction conditions in the contact zone between workpiece and tool are affected during the forming process, which has a significant influence on the material flow [15]. Nevertheless, only analytical and phenomenological approaches for mono materials have been published so far. Various research groups have investigated friction with regard to different oxide scale conditions which were induced by a defined furnace temperature and holding times in variable atmospheres. They showed that a thin oxide scale layer has a positive influence on the friction properties in contrast to thicker ones, which are harder and brittle [16–18]. Furthermore, there have been experimental investigations indicating a decrease of friction coefficient with increasing oxide scale layer thickness [19–21].

In addition, the forming behaviour of the steel matrix has a significant influence on the forging process. Parameters with a significant effect on the yield stress are process-specific parameters (e.g., strain rate and temperature) as well as material-specific parameters (e.g., alloying concept,

microstructure, and forming history) [22]. Experimental investigations have shown a significant influence of total carbon content on the material flow behaviour. An increase in carbon content has led to a reduction in the yield stress, particularly at high temperatures [23]. A Hensel–Spittel-based flow curve model which takes initial grain size, temperature, strain rate, and carbon content into account has been presented by Korpala et al. [24].

The main focus of the presented work is on the investigation of the oxide scale influence on the hot forging process, in particular on the plastic deformation and the material flow. Therefore, a numerical sensitivity analysis has been performed regarding the effect of oxide scale thickness, composition, and different friction conditions. This analysis is based on a numerical model for description of thin surface layers, which has been validated by means of an experimental ring compression test.

2. Materials and Methods

2.1. Experimental Procedure

The use of finite element FE-simulation requires detailed mathematical models for a realistic description of the material behaviour by consideration of process parameters like strain, strain rate, and temperature, as well as material-specific parameters like carbon content and initial grain size. Therefore, various experimental tests like the cylindrical compression test and the ring compression test have been performed. At least three repetitions have been performed for each experimental test.

The ring compression test is a standard procedure to investigate friction properties in forging processes. In the scope of this research project, ring compression tests have been performed in order to validate the numerical model as well as to determine the friction properties between the oxide scale layer and dies. The ring samples used had an outer diameter of 9 mm, an inner diameter of 4.5 mm, and a height of 3 mm. Figure 1a shows a deformed test sample. The experimental setup is provided in Figure 1b. After the ring compression test, the inner diameter and height were measured at different positions in order to calculate averaged values (Figure 1c).

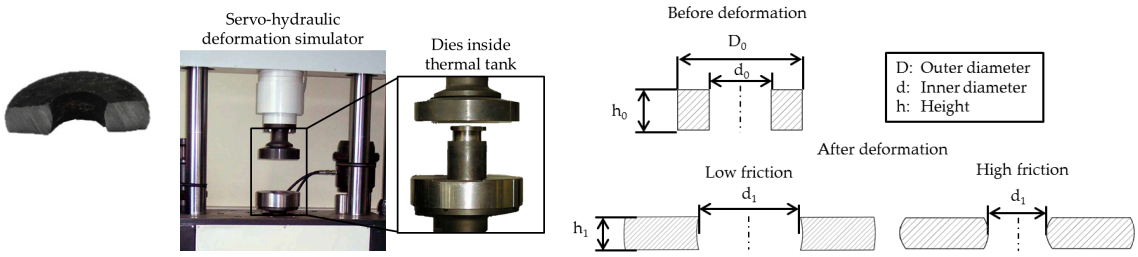

(**a**) (**b**) (**c**)

Figure 1. Deformed ring compression sample (**a**); Experimental ring compression setup on servo-hydraulic deformation simulator WUMSI with thermal tank (**b**); Schematic representation of ring compression test for different friction conditions (**c**).

The mechanical behaviour of different general steel grades with varying carbon content (C15, C45, C60) were examined by uniaxial compression tests. These unalloyed carbon steel grades were chosen in order to measure the influence of carbon content on forming behaviour as well as the growth of oxide scale layer without interference by other alloy elements. An overview of the chemical composition is shown in Table 1.

Table 1. Chemical composition of the steel samples in wt %.

Steel Grade	C	Si	Mn	P	S	Cr	Mo	Ni	Cu	Al
C15	0.160	0.210	0.420	0.001	<0.001	0.100	0.045	0.087	0.108	0.017
C45	0.490	0.200	0.420	0.001	0.001	0.100	0.034	0.081	0.096	0.021
C60	0.63	0.200	0.420	<0.001	<0.001	0.100	0.035	0.076	0.100	0.017

The used samples (diameter 10 mm, length 18 mm) showed a preformed and annealed initial microstructure. Within the experimental procedure, the samples were austenized at various temperatures and subsequently brought on different deformation temperatures. The experimental compression tests were performed on a servo-hydraulic deformation simulator (WUMSI, 400 kN, an in-house development of TU Freiberg, Germany and WPM Leipzig, Markkleeberg, Germany) with varying strain rates between 1 s^{-1} and 20 s^{-1}. The strain was measured by means of a linear variable differential transformer (LVDT) sensor which had been integrated into the cylinder. The tools made out of Al_2O_3 had been lubricated with graphite to reduce the influence of friction between the tools and the workpiece. An overview of the considered parameters is shown in Figure 2.

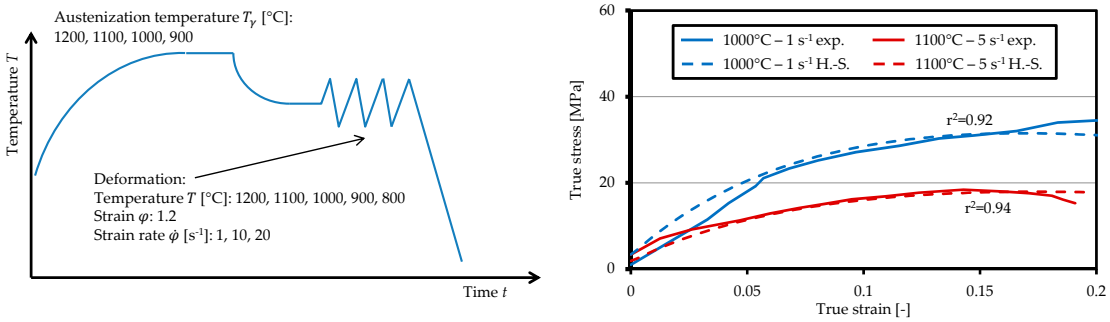

Figure 2. Schematic representation of the experimental procedure for the determination of flow curves for the steel matrix (**a**); Exemplary results of experimental cylindrical compression test and calculated true stress (H.-S.) for the pure iron oxide wuestite (based on [13]) (**b**).

Due to the fact that the mechanical properties of the iron oxides wuestite, magnetite, and haematite show a strong variation, separate flow curve models for each iron oxide were derived and parametrized based on the results of the experimental compression tests. In order to separately derive mechanical properties for each iron oxide, the required samples were manufactured with powder metallurgy. Therefore, pure oxide powders of haematite, magnetite, and wuestite were compressed and sintered into cylindrical samples. Subsequently, the samples were deformed in the temperature range of hot forming (900–1150 °C) and different strain rates up to 10 s^{-1}. Experimental results for the iron oxide wuestite at a temperature of 1000 °C and a strain rate of 1 $s^{-1,}$ as well as a temperature of 1100 °C and a strain rate of 5 s^{-1} are shown in Figure 2b. Detailed information regarding the powder metallurgy process route as well as experimental data for various temperatures and strain rates are presented in [13].

2.2. Aspects of the Numerical Model and Its Implementation

This paper focuses on the numerical investigation of thin oxide scale layers in a hot forging by the use of the finite element method. The developed numerical model is based on a multi-material approach in order to take the strongly varying mechanical properties of the steel matrix and the iron oxides in the oxide scale layer into account. Due to the fact that an experimental characterisation of the interface between oxide scale and steel matrix is very challenging, the contact between steel matrix and oxide scale surfaces is modelled as a glued contact type, which is similar to a tying

between node and surface. In order to reduce the computational time the 2D axial symmetry has been considered, the matrix as well as the oxide scale layer have been discretised with four-node, isoparametric, quadrilateral elements. The element stiffness is described by using four Gaussian points and a full integration scheme. The number of elements is about 20,000 but strongly depends on the oxide scale thickness. To avoid extensive element distortion, a remeshing criterion has been implemented. A schematic representation of the numerical model which had been set up in the commercial FE-software Simufact Forming v14.0.1 (Simufact Engineering Gmbh, Hamburg, Germany, 2017), which is based on the implicit MSC.Marc solver, is provided in Figure 3.

For a description of varying mechanical properties, the model is based on a multi-material approach. The calculation of actual yield stress with regard to the local temperature, strain, and strain rate, as well as material allocation, is carried out with a user subroutine which is scripted in FORTRAN with the FE solver. Each calculation process is linked with a specific element ID to ensure the correct assignment of calculated data to the correct numerical element. The user subroutine is called for each element in each iteration of every solver increment. The required data like local temperature, strain, and strain rate, as well as a material ID and element ID, are provided by the solver. Subsequently, the calculated yield stress is transferred back to the solver, linked with the specific element ID.

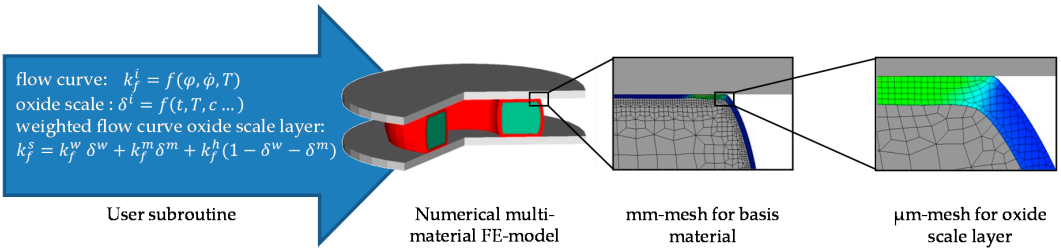

Figure 3. Schematic representation of the numerical model for thin surface layers and user subroutine.

In order to describe the thin surface layer consisting of three different materials, the oxide scale is considered to be a smeared continuum. Based on this approach, materials with non-uniform properties can be described as a homogenous continuum [25]. Therefore, single yield stresses are calculated for each of the iron oxides, wuestite, magnetite, and haematite, separately. For this purpose, three different material models parameterized with the findings of oxide scale characterisation are implemented as functions into the user subroutine. Each function calculates the flow stress for one of the three oxide scale parts depending on the current temperature, true strain, and strain rate, as well as material-specific parameters. With regard to the assumption of a smeared continuum, a weighting of the individual flow stresses is required in order to calculate a homogenous flow stress for the oxide scale layer. The weighted oxide scale flow stress is calculated depending on the oxide scale composition and is given by:

$$k_f^s = k_f^w\ \delta^w + k_f^m \delta^m + k_f^h(1 - \delta^w - \delta^m) \quad (1)$$

whereby k_f^s represents the global oxide scale flow stress, and k_f^w, k_f^m and k_f^h are the flow stress of the constituent oxide scale components. The terms δ^w and δ^h are the mass fractions of wuestite and magnetite, respectively. All numerical results of the oxide scale layer presented in this paper have been calculated based on the smeared approach described above and under assumption of various initial oxide scale compositions.

In general, the mass fractions depend on the temperature, time, and carbon content of the matrix material. Furthermore, within this common research project, an Arrhenius-based approach has been developed to describe the oxide scale growing process on carbon steel under consideration of carbon content [24]. This approach will be implemented into the user subroutine. A representation of the dataflow inside the user subroutine, as well as between the user subroutine and Simufact Forming solver, is given in Figure 4.

By integration of the user subroutine into the Simufact Forming GUI, key parameters like carbon content of used steel and oxide scale composition can be easily adjusted by the user. Due to the modular structure of the user subroutine, it can be easily extended to take other phenomena like separation of oxide scale parts into consideration.

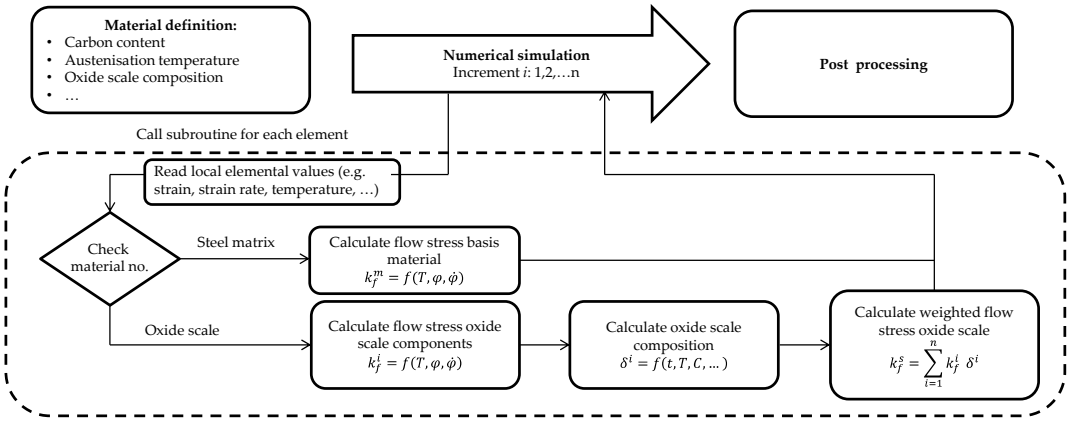

Figure 4. Dataflow inside the user subroutine as well as between the user subroutine and the numerical solver.

Based on experimental data, the models have been parameterized via regression analysis using the least square method. The onset of yielding is described by means of von Mises criterion. The plastic behaviour of the carbon steel (C15, C45, C60) is based on the following two Hensel–Spittel approaches according to [26]:

$$HS_a = A_a C\%^{m_{C_1}} \varphi^{m_a} e^{-m_{a1}\ T} \varphi^{m_{a2}\ \vartheta^{m_{a\varphi}}\ c\%^{m_{C_2}}}\ \dot{\varphi}^{m_{a3}} \tag{2}$$

$$HS_b = A_b C\%^{m_{C3}} e^{-m_{b1} T} \varphi^{m_{b2}} \dot{\varphi}^{m_{b3}} \tag{3}$$

The material hardening depending on temperature T, strain φ and strain rate $\dot{\varphi}$ at the beginning of the deformation process is described by the first term (HS_a) whereas the second term (HS_b) takes the material softening at higher strains caused by recrystallization into consideration. Both terms are weighted by a transition function δ:

$$\delta_{HS} = 0.5 + \pi^{-1} \tan^{-1} \left[w_1 T^{-w_2} (\varphi - \varphi_k T_\gamma^{w_\gamma} \dot{\varphi}^{w_4}) \right] \tag{4}$$

In addition to temperature, strain, and strain rate, this model takes into account the carbon content C as well as the initial grain size. Thus it is possible to describe various steel grades in a more general way regarding the concentration of the alloying element carbon. The initial grain size is considered with the help of austenization temperature T_γ, therefore the effect of preheating is also taken into account. An overview of the derived material-specific parameters A, m, w is presented in Tables 2 and 3.

Table 2. Material-specific parameters for the flow curve terms HS_a and HS_b.

A_a	m_{C_1}	m_{a1}	m_{a2}	$m_{a\varphi}$	m_{C_2}	m_{a3}	A_b	m_{C_3}	m_{b1}	m_{b2}	m_{b3}
3275	0.03662	0.0027	0.41618	−0.0421	−0.08004	0.07959	894	−0.01367	0.00276	0.00236	0.17777

Table 3. Material-specific parameters for the transition function δ_{HS}.

w_1	w_2	w_4	w_γ	φ_k
1.83501	0.00015	0.13325	0.048	0.15951

Exemplary calculated flow curves for the steels C15, C45, and C60 at various temperatures and a strain rate of 10 s^{-1}, using the approach for general steel, are presented in Figure 5a. Hereby, an austenization temperature of 1100 °C had been chosen. A comparison between experimentally-measured and calculated flow curves is shown for the steel grade C15 at different temperatures and a strain rate of 10 s^{-1} in Figure 5b. The comparison provides a good qualitative agreement. The calculated correlation coefficient (r^2) for the flow curve models is between 0.994 and 0.997. A validation for all steel grades has been presented in [24].

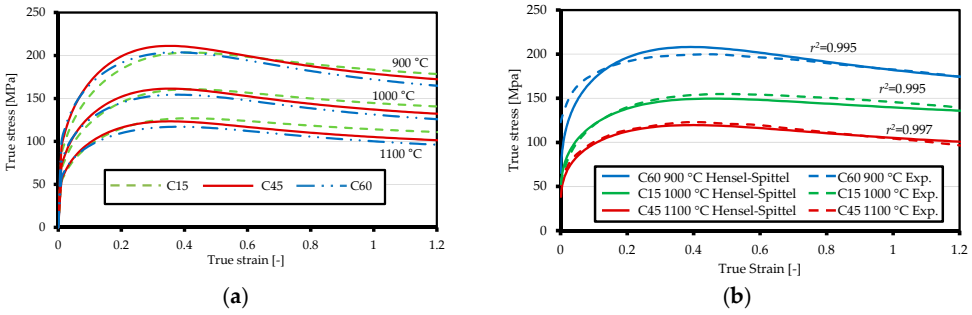

Figure 5. Calculated flow curves for the steel grades C15, C45, and C60 at different temperatures (900 °C, 1000 °C, 1100 °C) and a strain rate of 10 s^{-1} (a) Comparison between experimentally-measured and calculated flow curves for the steel grades C15, C45, and C60 at different temperatures and a strain rate of 10 s^{-1} (b).

The description of plastic behaviour of the iron oxides is based on Hensel–Spittel flow curve equations and thereby the current yield stress is expressed as a function of temperature, strain, and strain rate [13]. The flow curves have been parametrized based on the findings of cylindrical compression tests for the pure iron oxide samples. In the temperature range relevant for hot forging, the flow curves for the iron oxides, and in particular for wuestite, are lower in comparison with the calculated yield stresses of carbon steel. Exemplary calculated flow curves at a temperature of 1000 °C and various strain rates for the iron oxides wuestite, magnetite, and haematite are presented in Figure 6. An exemplary comparison between experimental data and calculated true stress based on the Hensel–Spittel (H.–S.) approach for the iron oxide wuestite is presented in Figure 2b. The calculated correlation coefficient (r^2) for all strain rates and temperatures is between 0.72 and 0.76 [13]. The variation of r^2 is due to the challenging experimental procedure for the pure iron oxides.

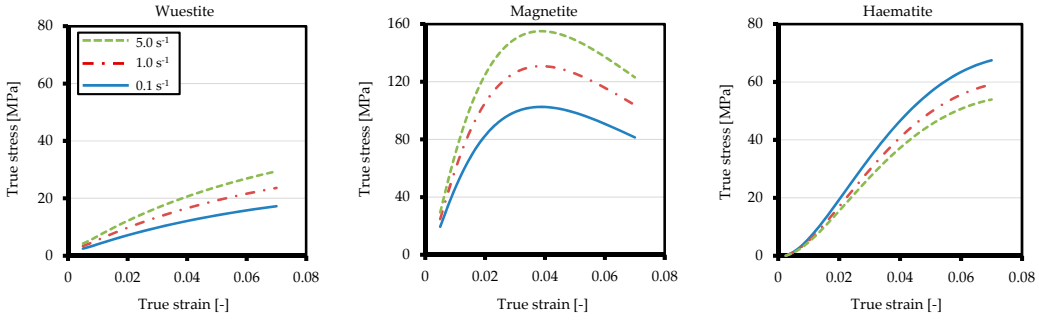

Figure 6. Exemplary calculated flow curves for wuestite, magnetite, and haematite at a temperature of 1000 °C.

3. Results and Discussions

3.1. Ring Compression Test and Model Validation

The presented numerical model has been validated by comparing numerical results with experimentally-measured force displacement curves of ring compression tests. Therefore, the samples

were heated to a temperature of 1000 °C and 900 °C with an oxidation time of 30 s. The preheating led to a specific oxide scale layer with an initial thickness of 50 µm, which had been used as an initial condition for numerical simulation. The initial thicknesses were measured on the basis of metallography recordings. Based on the findings of Tominaga [27] and Sun [28], an initial oxide scale composition of 64 wt % wuestite, 30 wt % magnetite, and 6 wt % haematite had been calculated for the oxidation temperature of 1000 °C. The dependency of oxide scale composition on oxidation temperature is shown in Figure 7, where the blue lines indicate the calculated composition at 1000 °C.

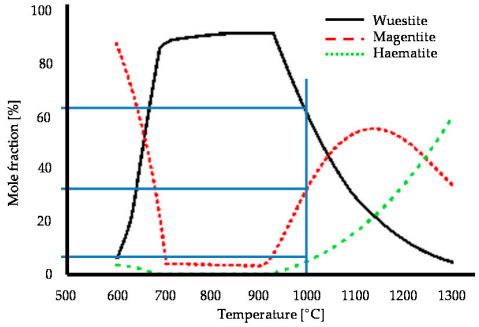

Figure 7. Oxide scale composition depending on oxidation temperature (based on [28]). The mole fractions for an temperature of 1000 °C are indicated by blue lines.

The heated sample was subsequently compressed with a stroke of up to 60% of its initial height. Due to the used isothermal containment, the tool temperature had been kept equivalent to workpiece temperature and the tools had been modelled as heat-conducting rigid bodies. The time–stroke relationship was calculated based on the experimental data with an average punch speed of 3.2 mm·s^{-1}. By evaluation of experimental ring compression tests, the friction factor (m) was found to be 0.65 (C15 and C60) and 0.7 (C45). For this purpose, the deformed samples had been geometrically measured and the ratios of initial inner diameter to deformed inner diameter as well as initial height to deformed height had been calculated and filled in a friction nomogram according to the work of Male and Cockcroft [29]. Experimental data for heat transfer coefficients were not measured in the current research project. Previous research studies predicted a heat transfer coefficient for non-fractured oxide scale which is 10–15 times lower than that of steel [30,31]. Based on these data, a heat transfer coefficient of 1400 W/(m^2·K) has been assumed for numerical simulation. A comparison of numerically-calculated and experimentally-measured force-displacement curves is presented in Figure 8a and shows a good qualitative agreement, thus it can be concluded that the used numerical boundary conditions are applicable.

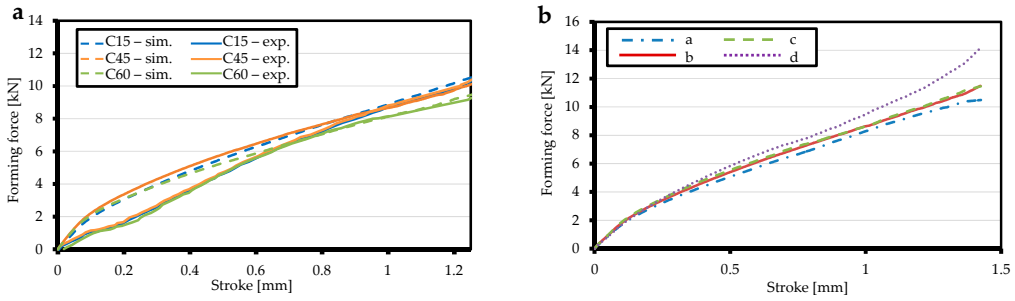

Figure 8. Comparison of experimentally-measured and numerically-predicted force-displacement curves for the steel grades C15, C45, C60 at a temperature of 1000 °C, an average forming speed of 3.2 mm s^{-1}, and the calculated ratio of 64:30:6 for the layers wuestite, magnetite, and haematite (**a**); Comparison of numerically-calculated force-displacement curves for the steel C15 at a temperature of 1000 °C, an average forming speed of 3.2 mm s^{-1}, and various ratios of haematite, magnetite, and wuestite a: 1:4:95; b: 6:30:64; c: 5:40:55 and d: without oxide scale. (**b**).

Particularly at the beginning of the forging process, there is an offset between measured and calculated force. This can be caused either by the machine stiffness in the experimental tests or due to the used oxide scale material model. On the basis of complex oxide scale material behaviour, the material characterisation had been examined to specific temperatures, strains, and strain rates. Therefore, the implemented flow curve model needs to be extrapolated for higher strains as well as a wider temperature range. Furthermore, in a complex hot forging process, the oxide scale is brittle and porous, thus it can be compressed and undergo rupture [13]. Subsequently, in order to examine the influence of a varying oxide scale composition, force displacement curves have also been calculated for different compositions of oxide scale as well as oxide scale (Figure 8b). The further boundary conditions have been kept unchanged. Although the mechanical properties of iron oxides differ widely, the global influence of oxide scale composition on force-displacement curve characteristics is small compared to the one without an oxide scale layer.

In addition to the comparison of force-displacement curves, the experimentally-measured and numerically-calculated inner diameters and heights after ring compression tests as well as the percentage deviation are presented in Table 4. The results show a good agreement.

Table 4. Comparison between experimentally-measured and numerically-calculated height and inner diameter after ring compression tests at 1000 °C and 900 °C.

Oxidation Temperature Oxide Scale Thickness	Steel Grade	Experimental (mm)		Simulation (mm)		Deviation (%)	
		Inner Diameter	Height	Inner Diameter	Height	Inner Diameter	Height
Oxidation temperature: 1000 °C Oxide scale thickness 50 µm	C15	3.7	1.61	3.91	1.63	5.1	1.2
	C45	3.75	1.67	3.86	1.7	2.9	1.8
	C60	3.8	1.68	3.77	1.66	−0.79	−1.2
Oxidation temperature: 900 °C Oxide scale thickness: 30 µm	C15	3.65	1.59	3.74	1.59	2.47	1.89
	C45	3.71	1.82	4.00	1.82	7.82	−1.1
	C60	3.8	1.67	3.81	1.68	0.26	0.6

3.2. Sensitivity Analysis

The numerical model presented in this paper was used to perform a sensitivity analysis regarding the influence of an oxide scale layer on the hot forging process. Therefore, influential parameters like layer thickness, friction conditions, and oxide scale composition have been studied. The carbon of the steel grade mainly influences the growth rate of the oxide scale layer. The mechanical behaviour of the oxide scale layer is regardless of the considered steel grade. Therefore, exemplary results for the steel grade C15 at 1000 °C are presented.

3.2.1. Layer Thickness

The growth of an oxide scale layer directly before or during the forming process is particularly influenced by oxidation time and temperature as well as the steel matrix. As the mechanical properties of oxide scale strongly deviate from the steel matrix, the forming process is influenced depending on oxide scale volume. The numerical simulations were carried out with ring compression samples and three different layer thicknesses (30 µm, 50 µm, 100 µm) as well as an unscaled variant. The further boundary conditions have been kept constant. Initially, a friction factor m = 0.65 had been assumed, derived from experimental ring compression tests for the steel grade C15.

The final ring profiles as well as the material flow in x-direction as contour plot are presented in Figure 9a. The impact of different oxide scale thicknesses on material flow and component shape can be seen between the oxide scaled variants and the variant without an oxide scale layer as well as between the scaled variants themselves. The variant without an oxide scale layer shows a conventional material flow, known from the ring compression test with high friction. The material flow is divided and the change of inner diameter is related to the friction conditions, whereby the sides form a convex shape. With an increasing friction factor, the decrease of the inner diameter is intensified [32]. However,

the scaled variants show a light concave up to a straight shape at the inner diameter, which increases with increasing layer thickness. The shape at the outer diameter turns from slight convex to a flat surface with increasing layer thickness. The numerical results indicate an increased sliding behaviour in the contact zone of workpiece and die as a result of the oxide scale, which leads to changes in friction conditions and material flow. The oxide scale layer seems to act like an additional lubricant, whereby the effect is intensified with increasing layer thickness. It can be assumed that the yield stresses of the oxide scale and the steel matrix decisively differ and thus provoke the changes in material flow as well as an increased sliding. Furthermore, the different yield stresses result in an outflow of the oxide scale in the contact zone between the die and the steel matrix.

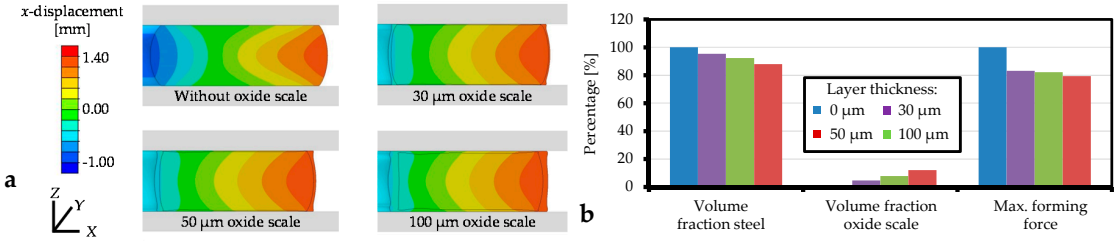

Figure 9. Final component shape and x-displacement depending on oxide scale thickness (**a**); influence of oxide scale on maximum forming force (**b**).

The volume fractions of steel matrix, oxide scale, and the maximum forming forces are shown as percentages in Figure 9b. The bar chart shows the influence of thin oxide scale layers as well. The volume fraction of a 50-µm oxide scale layer is just about 10% but results in a forming force reduction of nearly 20%. This strong reduction at even small amounts of oxide scale is not just due to lower yield stresses of the oxide scale. It indicates an improved sliding as well. Nonetheless, it must be taken into account that the results are calculated based on the approach of non-fractured oxide scale. In complex forging processes, the oxide scale can rupture due to its brittleness, which also has an influence on sliding behaviour. Therefore, it is necessary to implement a specific damage criteria into the user subroutine in order to take into account rupture of oxide scale as well as oxide scale detachment. Furthermore, new material characterisation methods are required in order to measure rupture as well as the detachment of the thin and brittle oxide scale layer at elevated temperatures, which might be more challenging.

3.2.2. Friction Conditions

In order to carry out further examinations on the influence of oxide scale on the sliding behaviour in the contact zone between workpiece and die, additional simulations for a variant without oxide scale and a variant with an oxide scale layer of 50 µm at 1000 °C have been performed while varying the friction factor m. Calculated results for the final component shape and material flow in *x*-direction for three variants with and without oxide scale and a varying friction factor are shown in Figure 10.

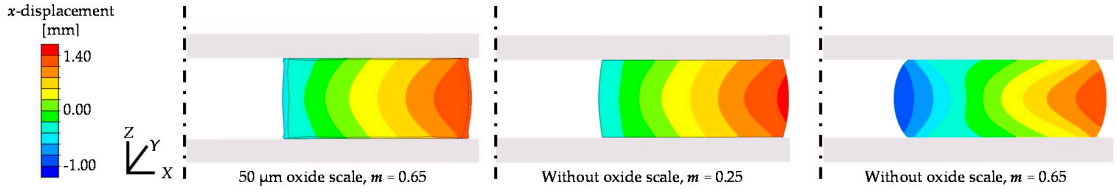

Figure 10. Final component shape and *x*-displacement depending on the friction factor *m* and the oxide scale.

The results clarify the assumptions of an improved sliding behaviour due to oxide scale. The variant without an oxide scale layer and a very low friction factor of m = 0.25 shows an almost identical final shape to the variant with oxide scale and a friction factor of m = 0.65. The material flow also shows a relatively good agreement, whereby a higher flow is observed for the variant without oxide scale. The calculated force–displacement curves of the variants mentioned above are presented in Figure 11. A comparison between the variant without oxide scale considering m = 0.25 and the variant with oxide scale considering m = 0.65 shows a good qualitative agreement compared to the variant without oxide scale and m = 0.65. Thus it can be assumed that the oxide scale reduces the friction and acts like a lubricant.

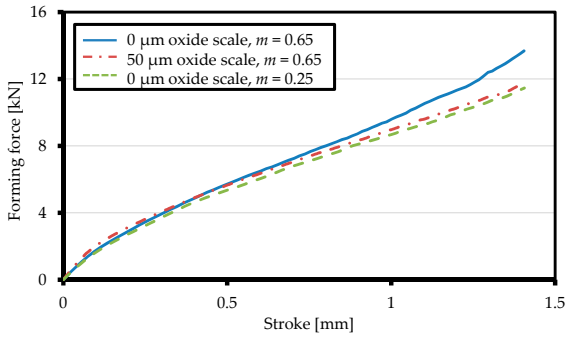

Figure 11. Numerically-calculated force–displacement curves for ring compression tests of variants with and without oxide scale for different friction factors.

In addition, further numerically-calculated variants with and without oxide scale and varying friction factors (low, medium, high friction) are compared in Figure 12 to point out the effect of the oxide scale presence on the sliding behaviour. The variants without oxide scale show, as expected, a decreasing inner diameter and increasing material flow inwards with increasing friction factor. Only the variant with low friction (m = 0.1) shows a concave shape at the inner diameter. However, only the scaled variant with high friction (m = 0.85) exhibits a decreased inner diameter as well as a concave shape. All scaled variants show an intensified material flow outwards, as compared with the variants without oxide scale. Thus, the oxide scale seems to dampen the friction influence.

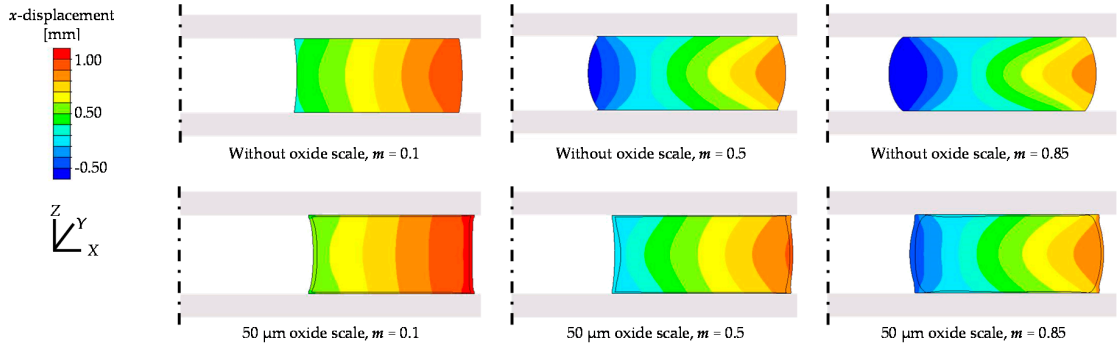

Figure 12. Comparison between numerically-calculated variants with and without oxide scale and varying friction.

3.2.3. Oxide Scale Composition

The composition of an oxide scale layer changes depending on the process and material-specific parameters like oxidation time and temperature. Due to the fact that mechanical properties of iron oxides strongly deviate from each other, the forming process is influenced by their composition.

The final component shape as well as calculated v. Mises stresses are presented in Figure 13 with regard to varying oxide scale compositions.

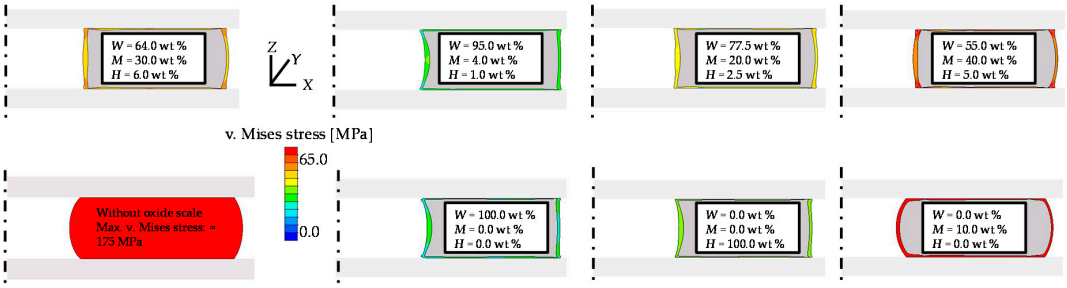

Figure 13. Final component shape and v. Mises stress depending on mass fractions of wuestite (*W*), magnetite (*M*), and haematite (*H*).

Four variants with different combinations of the iron oxides and a thickness of 50 µm as well as one variant without oxide scale were calculated. Additionally, three variants with pure oxides (wuestite, magnetite, haematite) were calculated. The further boundary conditions have been kept constant. The calculated v. Mises stress inside the steel matrix was higher than inside the oxide scale layer regardless of the oxide scale composition. The variant, with a layer consisting of 100 wt % magnetite, exhibited the highest v. Mises stress as compared with the other pure oxide variants. Furthermore, a strong influence of oxide scale composition on resulting stresses can be seen. A reduction of wuestite mass fraction or increase of the mass fractions of magnetite and haematite led to an increase of stresses inside the oxide scale layer. This clarifies the above-mentioned strong variations of oxide scale mechanical properties. The influence on material flow as well as sliding behaviour was reduced by an increase of yield stresses of oxide scale and the accompanying alignment with the steel matrix. The variant with the lowest mass fraction of wuestite and highest v. Mises stresses showed the lowest deviations of final shape as compared to the variant without oxide scale.

Furthermore, experimental and numerically-calculated height and inner diameter after compression have been determined under consideration of varying oxide scale composition. An overview is shown in Table 5. The variants with different oxide scale compositions exhibited a strong variation of resulting inner diameter which is consistent with the assumption that the oxide scale itself and the composition influence the material flow. The variant with the highest mass fraction of haematite showed the closest agreement with experimentally-measured values. The differences between the experimentally-measured and numerically-calculated values could have been caused by sliding of the oxide scale on the steel matrix as well as fracture. In this regard, further experimental investigations on the oxide scale composition have to be carried out.

Table 5. Experimental and numerically-calculated height and inner diameter after ring compression tests for the variants with steel grade C15 at a temperature of 1000 °C.

Variant	Height (mm)	Inner Diameter (mm)
Experimental ring compression test (averaged)	1.62	3.7
Simulation; *W* = 64.0 wt %; *M* = 30.0 wt %; *H* = 6.0 wt % (calculated composition for 1000 °C based on [28])	1.63	3.91
Simulation; *W* = 55.0 wt %; *M* = 40.0 wt %; *H* = 5.0 wt %	1.63	3.89
Simulation; *W* = 77.50 wt %; *M* = 20.0 wt %; *H* = 2.5 wt %	1.63	4.25
Simulation; *W* = 95.0 wt %; *M* = 4.0 wt %; *H* = 1.0 wt %	1.63	4.41
Simulation; without oxide scale	1.62	2.67

4. Conclusions

Based on a multi-material approach, an FE-model describing the oxide scale material behaviour in hot forging has been developed. Four different material models for both oxide scale and steel have been implemented in Simufact Forming by means of user subroutines. This enables an accurate description of the oxide scale material flow behaviour depending on temperature, strain, and strain rate. Furthermore, the implemented model for general steel grades takes into account the influence of varying carbon content as well as the initial microstructure. The influence of carbon content on the yield stress can be seen in the Hensel–Spittel coefficients. However, no significant influence of carbon content on the forming behaviour has been identified. The developed numerical model has been validated by comparing the results of the performed ring compression tests and the numerical simulation. Within a numerical sensitivity study, influential parameters of oxide scale layer like layer thickness, friction behavior, and oxide scale composition have been variated. The numerical results show a decisive influence of the oxide scale layer on a hot forging process. The comparison of variants with and without an oxide scale shows that the presence of an oxide scale layer in the contact zone between die and steel matrix acts like an additional lubricant. The findings indicate that, beside others, the differences between yield stress in steel matrix and oxide scale layer lead to an improved sliding behaviour. Nevertheless, it must be taken into account that the results are calculated based on the approach of non-fractured oxide scale. Therefore, further investigations on the adhesion interface between oxide scale and metal matrix as well as oxide scale rupture will be carried out in order to examine its behaviour during the hot forging process. For this purpose, the presented user subroutine will be extended with a damage criteria. This will enable more detailed description of the oxide scale influence on the hot forging process.

Acknowledgments: This work was part of the cooperation project "General modelling of material behaviour and surface modifications for FEM analysis of die forging of carbon steels" (GR4872/1-1, UL471/1-1, BO3616/10-1) funded by the German Research Foundation (DFG). The authors would like to thank the DFG for its financial support.

Author Contributions: Rudolf Kawalla, Grzegorz Korpala and Madlen Ullmann designed and performed the experiments for general steel; Birgit Awiszus and Marcel Graf designed and performed the experiments for iron oxides; Bernd-Arno Behrens, Alexander Chugreev and Hendrik Wester designed the numerical model and implemented subroutines as well as performed the sensitivity analysis; Hendrik Wester wrote the paper.

Conflicts of Interest: The authors declare no conflict of interest.

References

1. Fischer, M.U.A.; Dickert, H.H.; Bleck, W.; Huskic, A.; Kazhai, M.; Hadifi, T.; Bouguecha, A.; Behrens, B.-A.; Labanove, N.; Felde, N.; et al. EcoForge: Energieeffiziente Prozesskette zur Herstellung von Hochleistungs-Schmiedebauteilen. *HTM J. Heat Treat. Mater.* **2014**, *69*, 209–219. (In German) [CrossRef]
2. Luong, L.; Heijkoop, T. The influence of scale on friction in hot metal working. *Wear* **1981**, *71*, 93–102. [CrossRef]
3. Behrens, B.-A.; Bouguecha, A.; Vucetic, M.; Chugreev, A. Advanced wear simulation for bulk metal forming processes. In Proceedings of the Numiform 2016: The 12th International Conference on Numerical Methods in Industrial Forming Processes, Troyes, France, 4–7 July 2016; Volume 80. [CrossRef]
4. Behrens, B.-A. Finite element analysis of die wear in hot forging processes. *CIRP Ann. Manuf. Technol.* **2008**, *57*, 305–308. [CrossRef]
5. Kawalla, R.; Steinert, F. Untersuchung des Einflusses von Prozessparametern in der Fertigstraße auf die Tertiärzunderausbildung. *Mat.-wiss. u. Werkstofftech.* **2007**, *38*, 36–42. [CrossRef]
6. Krzyzanowski, M.; Beynon, J.; Farrugia, D. *Oxide Scale Behavior in High Temperature Metal Processing*; Wiley-VCH Verlag GmbH & Co. KGaA: Weinheim, Germany, 2010; ISBN 978-35-2-732518-4.
7. Malik, A.U.; Whittle, D.P. Oxidation of Fe-C alloys in the temperature range 600–850 °C. *Oxid. Met.* **1981**, *16*, 339–353. [CrossRef]
8. Birks, N.; Frederik, S.; Meier, G.H. *Introduction to High Temperature Oxidation of Metals*, 2nd ed.; Cambridge University Press: Cambridge, UK, 2006; ISBN 978-05-2-148517-3.

9. Kubaschewski, O.; Hopkins, B.E. Oxidation of metals and alloys. *Mater. Corros.* **1954**, *11*, 108–114. [CrossRef]
10. Brauns, E.; Rahmel, A.; Christmann, H. Die Verschiebung des Nonvarianzpunktes zwischen Eisen, Wüstit, Magnetit und Sauerstoff im System Eisen—Sauerstoff durch Legierungselemente oder fremde Oxyde—Auswirkungen auf das Verhalten von Eisenlegierungen beim Verzundern. *Arch. Eisenhttenwes.* **1959**, *30*, 553–564. [CrossRef]
11. Garnaud, G.; Rapp, R.A. Thickness of the oxide scale layers formed during the oxidation of iron. *Oxid. Met.* **1977**, *11*, 193–198. [CrossRef]
12. Graf, M.; Kawalla, R. Scale behaviour and deformation properties of oxide scale during hot rolling of steel. *Key Eng. Mater.* **2012**, *504–506*, 546–551. [CrossRef]
13. Graf, M. *Modellierung des Zunderverhaltens Entlang der Prozesskette Warmband, TU Bergakademie Freiberg*; Freiberger Forschungsheft B353: Freiberg, Germany, 2013; ISBN 978-38-6-012480-2.
14. Takeda, M.; Onishi, T.; Nakakubo, S.; Fujimoto, S. Physical properties of iron-oxide scales on Si-containing steels at high temperature. *Mater. Trans.* **2009**, *50*, 2242–2246. [CrossRef]
15. Behrens, B.-A.; Bouguecha, A.; Hadifi, T.; Mielke, J. Advanced friction modeling for bulk metal forming processes. *Prod. Eng.* **2011**, *5*, 621–627. [CrossRef]
16. Barnes, D.J.; Wilson, J.E.; Stott, F.H. The influence of oxide films on the friction and wear of Fe-5% Cr alloy in controlled environments. *Wear* **1977**, *45*, 161–176. [CrossRef]
17. Vergne, C.; Boher, C.; Gras, R.; Levailant, C. Influence of oxides on friction in hot rolling: Experimental investigations and tribological modelling. *Wear* **2000**, *260*, 957–975. [CrossRef]
18. Hinsley, C.F.; Male, A.T.; Rowe, G.W. Frictional properties of metal oxides at high temperatures. *Wear* **1968**, *11*, 233–238. [CrossRef]
19. Munther, P.A.; Lenard, J.G. The effect of scaling on interfacial friction in hot rolling of steels. *J. Mater. Process. Technol.* **1993**, *37*, 3–36. [CrossRef]
20. Tingle, E.D. The importance of surface oxide films in the friction and lubrication of metals. *Trans. Faraday Soc.* **1950**, *46*, 93–102. [CrossRef]
21. Matsumoto, R.; Osumi, Y.; Utsunomiya, H. Reduction of friction of steel covered with oxide scale in hot forging. *J. Mater. Process. Technol.* **2014**, *214*, 651–659. [CrossRef]
22. Graf, M.; Ullmann, M.; Korpalla, G.; Kawalla, R. Materialkennwerte als Basis für die nummerische simulation von Warmumformprozessen. In Proceedings of the 22. Verformungskundliches Kolloquium, Planneralm, Germany, February 2013; pp. 49–55.
23. Wray, P.J. Effect of carbon content on the plastic flow of plain carbon steels at elevated temperatures. *Metall. Trans. A* **1982**, *13*, 125–134. [CrossRef]
24. Korpała, G.; Ullmann, M.; Graf, M.; Wester, H.; Bouguecha, A.; Awiszus, B.; Behrens, B.-A.; Kawalla, R. Modelling the influence of carbon content on material behavior during forging. *AIP Conf. Proc.* **2017**, *1896*, 190013. [CrossRef]
25. Behrens, B.-A.; Kawalla, R.; Awiszus, B.; Bouguecha, A.; Ullmann, M.; Graf, M.; Bonk, C.; Chugreev, A.; Wester, H. Numerical investigation of the oxide scale deformation behaviour with consideration of carbon content during hot forging. *Procedia Eng.* **2017**, *207*, 526–531. [CrossRef]
26. Korpala, G. *Einfluss der Chemischen Zusammensetzung auf die Mechanischen Eigenschaften von Unlegiertem Bainitischen Stahl mit Restaustenit*; Freiberger Forschungshefte: Freiberg, Germany, 2016.
27. Tominaga, J.; Wakimoto, K.; Mori, T.; Murakami, M.; Yoshimura, T. Manufacture of wire rods with good descaling property. *Trans. Iron Steel Inst. Jpn.* **1982**, *22*, 646–656. [CrossRef]
28. Sun, W. A Study on the Characteristics of Oxide Scale in Hot Rolling of Steel. University of Wollongong Thesis Collection. 2005. Available online: http://ro.uow.edu.au/theses/440 (accessed on 13 February 2018).
29. Male, A.T.; Cockcroft, M.G. A method for the determination of the coefficient of friction of metals under conditions of bulk plastic deformation. *J. Inst. Met.* **1964**, *93*, 38–46.
30. Krzyzanowski, M.; Beyon, J.H. Oxide Behaviour in hot rolling. In *Metal Forming Science and Practice*; Lenard, J., Ed.; Elsevier: Amsterdam, the Netherlands, 2002; pp. 259–295. ISBN 978-00-8-053631-6.

31. Frolish, M.F.; Krzyzanowski, M.; Beyon, J.H. Oxide scale behaviour on aluminium and steel under hot working conditions. *J. Mater. Process. Technol.* **2006**, *177*, 36–40. [CrossRef]
32. Koch, S.; Vucetic, M.; Hübner, S.; Bouguecha, A.; Behrens, B.-A. Superimposed oscillating and non-oscillating ring compression tests for sheet-bulk metal forming technology. *Appl. Mech. Mater.* **2015**, *794*, 89–96. [CrossRef]